An Euler-Lagrange Approach to Model the Dynamics of Particulate Phase Exposed to Hot Gas Injection into Packed Bed Reactors

E. Rabadan Santana[1,a)] and B. Peters[1]

[1]Research Unit of Engineering Science RUES, University of Luxembourg, Luxembourg

[a)]Corresponding author: edder.rabadan@uni.lu

ABSTRACT

In the present work a coupled Euler-Lagrange approach is used to model the dynamics of a particulate phase and its interaction with hot gas injection into particle bed reactors. The proposed numerical approach is based on the Discrete Element Method (DEM) to model the granular phase. The in-house DEM solver has been extended to account for heat and mass transfer within the gas phase by coupling it with the governing Navier-Stokes equations in the Eulerian Computational Fluid Dynamics (CFD) gas model. This coupling has been done by using the CFD OpenFoam library. As a result the numerical simulation framework called the Extended Discrete Element Method (XDEM) has being developed. The present case uses the XDEM as a numerical tool to study a generic small scale packed bed reactor where hot gas is injected laterally into a packed bed of coke particles. The interaction between solids and different fluid phases in packed bed reactors represents a challenging phenomenon for numerical simulation. In order to represent more accurately such processes the XDEM code has being adapted and several features like particle gasification, chemical reaction and diverse particle shapes have been implemented. The XDEM Euler-Lagrange approach showed the ability to track the positions of the coke particles in the simulation domain allowing an in-depth study of the particle-gas interaction. Since hot air at 1200 K was injected, the effects of gasification, reactions inside the particles, and shrinking were considered. Comparison between measured and predicted data was made for char coal particles.

Keywords: Extended Discrete Element Method, Euler-Lagrange, Hot Blast, Packed Bed, Gas-Particle interaction, Gasification.

Introduction

Injection of preheated air at high speed or blast injection is being used extensively in many industrial applications such as packed bed reactors. When air is injected laterally into a particle bed it causes the formation of granular circulation region within the bed. This process increases the interaction between the solid and gas phases resulting in a more efficient heat and mass transfer within the reactor. Blast injection is widely use in different petrochemical and metallurgical processes such as catalyst, gasification, and combustion. One of the main applications of blast injection is found in the Blast Furnace (BF) reactors. Blast furnace reactors are widely used in the ironmaking industry and are one of the largest operational reactors. Typical dimensions of BF area about 40 m high and 15 m wide for a production over 10 000 t/d of pig iron [1]. The nature of the blast furnace operation includes several types of flow, a packed bed of solids descending, liquid dripping and gas with powder ascending through the packed bed [2]. In a BF liquid iron is produce from ferrous oxides and carbon reductants. Ore is normally used as a ferrous oxide and coke as a carbon reductant. Ore and coke are charged in layers from the top of the furnace. At the bottom part of the furnace, hot air is injected at high velocity through a tuyere. The fast stream of blast gas entering into the packed bed forces the coke particles to displace back and upwards forming a circulation region around the injected gas. This circulation zone forms a cavity called raceway. A schematic drawing of the blast furnace and the raceway are shown in Fig. 1. In the raceway the carbon from the coke or other auxiliary fuels for instance the pulverized coal (PC) reacts with the oxygen to provide heat and to form the main reductant gas, CO. The reductant gas rises through the void space towards the top of the furnace. Chemical reactions take place as the solid material moves downward and interacts with the reductant gas producing liquid iron and carbon dioxide. The final products in form of melted iron and slag are tapped from the bottom of the blast furnace and the flue gas is removed from the top.

Since the stability of the BF operation is related to the motion of coke particles in and around the raceway, many studies have been conducted focusing on the gas flow and the formation of the cavity [4, 5]. However, modeling the raceway

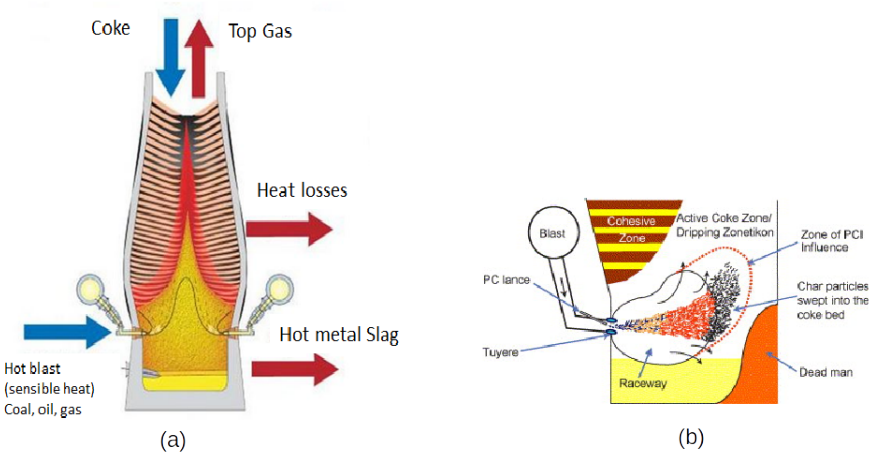

Figure 1: (a) General scheme of a blast furnace [2]; (b) the raceway [3].

is a challenging task due to the high velocities of the blast gas and its interaction with the particles, existence of high temperatures, chemical reactions, and shrinkage of particles [1, 6]. Currently, two models are used to investigate the in-furnace phenomena: continuum model and Discrete Element Method (DEM). In the first approach the geometry/shape of the raceway is fixed and the bed of coke is consider to be a porous media. In such approach the Navier-Stokes equations accounting for porosity are solved over the entire domain [7, 8]. This method is restricted to the dynamics of the gas flow therefore, the formation of the raceway cannot be investigated. Consequently, is not possible to determine the boundaries of the raceway. In the second approach, the Discrete Element Method (DEM), the solid phase is considered as a discrete part while the flow (liquid and/or gas) in the void space between the particles is treated as a continuum phase. This approach also referred to as the Combined Continuum and Discrete Model (CCDM) [9] can be able to predict the distribution of the particulate phase under the influence of lateral gas injection.

In the present work the developed simulation framework *Extended Discrete Element Method (XDEM)* is used to model the motion of the particulate phase and its interaction within the gas. For that purpose, an over-simplified geometry of a generic packed bed reactor is used to evaluate the XDEM. The geometry includes lateral gas injection, as in the case of BF reactors. However, at this stage, the intention of this work is to study the Euler-Lagrange approach of the XDEM to model such type of solid-flow configurations and not the in-furnace phenomena. In a next step, simulations with more realistic geometries and operational conditions have to be conducted to address the in-furnace phenomena.

Numerical Framework: the eXtended Discrete Element Method (XDEM)

The proposed numerical approach is based on the Discrete Element Method (DEM) to model the dynamics of granular matter and the Eulerian Computational Fluid Dynamics (CFD) model for the fluid phase. A coupling between both modeling approaches allows to track the individual motion of the particles and the dynamics of the fluid phase. For that purposes, the in-house DEM solver has been coupled with the open source library OpenFoam. The coupling between both solvers resulted in the development of the numerical simulation framework called the eXtended Discrete Element Method (XDEM) [10]. As a result the XDEM solver accounts for heat and mass transfer within the solid and fluid phases. Within the XDEM solver, the CFD gas phase is solved using OpenFoam. The coupling algorithm between the in-house DEM solver and OpenFoam allows to exchange information between the discrete and gas phases at each time step. In this way, the current position of individual particles can be tracked. In addition, particles are allowed to exchange heat and mass transfer with its environment. This allows to determine, for each particle, its temperature, porosity, reaction degree, shrinking, and species distribution in conjunction with the surrounding gas phase.

A schematic representation of the XDEM modular structure is showed in Fig. 2. The XDEM is composed by two modules: dynamics and conversion modules. The Lagrangian concept of the XDEM-Dynamics module is used to predict the motion of solid particles. The movement of particles is characterized by the motion of a rigid body through six degrees of freedom for translation along the three directions in space and rotation about the centre-of-mass. Thus, the entire motion of each particle is describe by these degrees of freedom. This method is widely accepted and effective to address engineering problems in granular and discontinuous materials, especially in granular flows, rock mechanics, and powder mechanics

[11, 12, 13, 14]. Chemical conversion at each discrete particle is computed by the XDEM-Conversion module. A discrete particle may consist of different phases like solid, liquid, gas or inert material. Since particles can be porous, gas diffusion within the pore volume is accounted for. A particle is allowed to exchange heat with its environment depending on the specified boundary conditions for its surrounding gas. The distribution of temperature is accounted for by system of one dimensional and transient conservation equations for energy [15, 16]. For the particle energy balance, local thermal equilibrium between gas phase and the porous solid is assumed. Thermal energy is transferred from the fluid to the particles and/or from particles to fluid as a heat source. The XDEM-Conversion calculates for each CFD cell the corresponding heat source value depending on the particles properties within the specific cell. The modular structure of the XDEM allows to use the dynamics and conversion modules in a de-coupled mode for better adaptability to the modeling requirements [17]. Figure 2 shows the modular structure of the XDEM solver.

For the present case-study all modules of the XDEM including the coupling with the CFD tool are used. The gas phase is modeled in an Eulerian approach solving the Navier-Stokes equations for compressible fluid in porous media implemented in OpenFoam. The position, orientation, and heat interaction between particles (conduction, radiation) as well as between particles and their environment (conduction, convection) is resolved with the above mentioned XDEM modules.

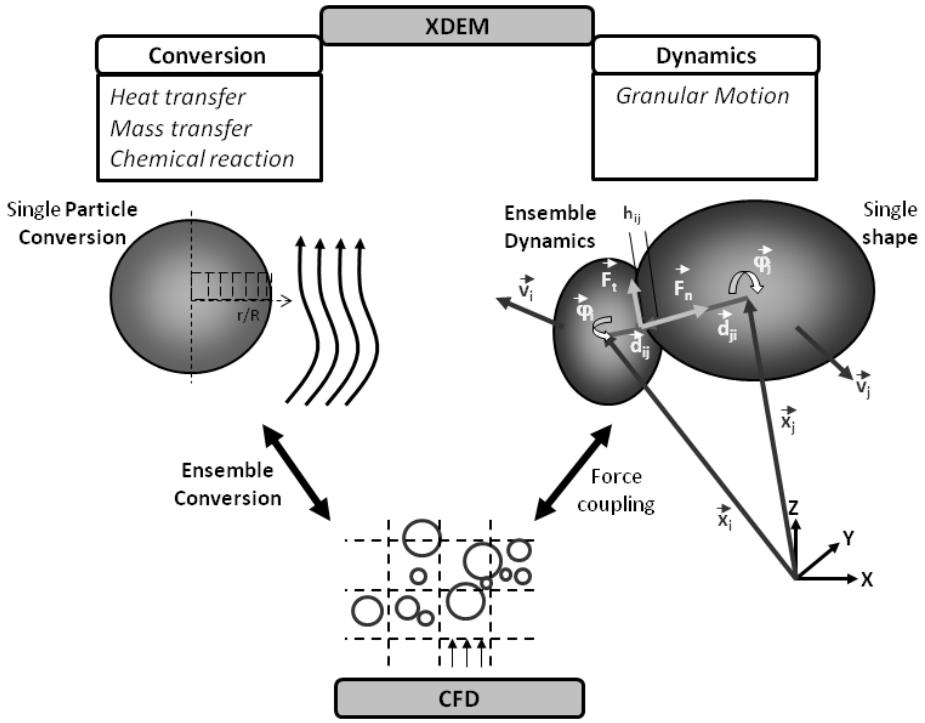

Figure 2: Interaction modules in the XDEM.

The complete set of equations and detailed description of the XDEM numerical framework can be found in [18, 10, 16]. For purpose of clarity a brief description of the main equations is given next. Heat interaction between particles as well as heat and mass transfer between particles and their environment is solved with the XDEM-Conversion module. Thus, the conservation equations of mass, momentum, energy, and species are solved for a porous particle:

$$\frac{\partial(\epsilon_p \rho_f)}{\partial t} + \nabla \cdot \left(\epsilon_p \rho_f v_f\right) = \dot{m}_{s,f} \tag{1}$$

$$-\frac{\partial(\epsilon_p p)}{\partial x} = \frac{\mu_f \epsilon_p}{K} v_f \tag{2}$$

$$\frac{\partial(\rho c_p T)}{\partial t} = \frac{1}{r^n}\frac{\partial}{\partial r}\left(r^n \lambda_{\text{eff}} \frac{\partial T}{\partial r}\right) + \sum_{k=1}^{l} \dot{\omega}_k H_k \tag{3}$$

$$\frac{\partial(\epsilon_p\,\rho_{f,i})}{\partial t} + \nabla\cdot\left(\epsilon_p\,\rho_{f,i}\,v_f\right) = \frac{1}{r^n}\frac{\partial}{\partial r}\left(r^n\epsilon_p D_i\frac{\partial\,\rho_{f,i}}{\partial r}\right) + \dot{m}_{s,f,i} \tag{4}$$

The term on the right hand side in the mass conservation equation, Eq. (1), accounts for the mass transfer between the fluid within the pore of the particle or the solid phase with gas as a result of the chemical reactions, ϵ_p denotes the particle porosity, v_f the advective velocity, and ρ_f the density of the gas phase. Equation (2) is the momentum equation based on Darcy's law for the transport of gaseous species within the pore space of the particle; here K represent the permeability, p the pressure, and μ the dynamic viscosity. Since the thermal mass in the solid and fluid phase are significantly greater than the thermal mass in the gas phase (ρc_p), the heat transported through the bulk motion or diffusion of the gaseous species within the pore space can be neglected. Thus, the energy balance equation, Eq.(3), is based on the homogeneous model for a porous medium as described by Faghri [19] where λ_{eff} is the effective thermal conductivity evaluated as [20]

$$\lambda_{\text{eff}} = \epsilon_p\lambda_f + \sum_{i=1}^{k}\eta_i\,\lambda_{i,solid} + \lambda_{rad} \tag{5}$$

which takes into account heat transfer by conduction in the gas, solid, and radiation in the pore. The later is evaluated as

$$\lambda_{rad} = \frac{\epsilon}{1-\epsilon}\,\sigma\,4.0T^3 \tag{6}$$

where T and σ stand for the temperature and the Boltzmann constant, respectively. The source term $\dot{\omega}$ represents the production or consumption of heat due to chemical reactions where H_k is the enthalpy of reaction k. The formulation of Eq. (3) allows to represent different geometries based on a radial coordinate r: infinite plate ($n = 0$), infinite cylinder ($n = 1$), and sphere ($n = 2$). Equation (4) is the conservation equation of species which accounts for convection in conjunction with diffusive transport to describe the distribution of gaseous species i in the porous particle. The effective diffusion coefficient $D_{i,\text{eff}}$ of species i is derive from the influence of tortuosity τ and the molecular diffusion coefficient D_i [21, 22]:

$$D_{i,\text{eff}} = D_i\frac{\epsilon_p}{\tau} \tag{7}$$

Depending on the rate-limiting process, the depletion of the solid material results in either a decreasing particle density or a reduction of the particle size [23, 24]. The distribution of the porosity and the specific inner surface S are determined by the following equations:

$$\frac{\partial\epsilon}{\partial t} = \frac{M}{\rho\delta}\dot{\omega} \tag{8}$$

$$\frac{\partial S}{\partial t} = \frac{1-\epsilon_0}{C_0}\dot{\omega} \tag{9}$$

where M is the molecular weight of the particle, δ is the characteristic pore length and C_0 and $\dot{\omega}$ are the concentration and reaction of the solid material, respectively. The subindex 0 indicates the initial values of the appropriate variable.

Since geometries are consider to be either infinite plate, infinite cylinder or sphere, a symmetric boundary condition is applied at the center of the particle for the effective thermal conductivity

$$-\lambda_{\text{eff}}\frac{\partial T}{\partial r}\bigg|_{r=0} = 0 \tag{10}$$

and for the heat and mass transfer at the surface of the particle

$$-\lambda_{\text{eff}}\frac{\partial T}{\partial r}\bigg|_{r=R} = \alpha(T_R - T_\infty) + \dot{q}_{\text{rad}} + \dot{q}_{\text{cond}} \tag{11}$$

$$-D_{\text{i,eff}}\frac{\partial\rho_i}{\partial r}\bigg|_{r=R} = \beta_i(\rho_{i,R} - \rho_{i,\infty}) \tag{12}$$

where T_∞ is the gas temperature, $\rho_{i,\infty}$ the ambient density, D_i, α_i and β_i are the diffusion, heat, and mass transfer coefficients of species i, respectively. The heat fluxes $\dot{q}''$ in Eq. (12) account for potential radiative heat exchange with the surrounding and/or conductive heat transport through physical contact with other bodies. Thermodynamic equilibrium within the intra-particle fluid is assumed and the thermal equation of state is used to close the above set of equations $p = \rho RT$ and $h = c_pT$, both used in their formulation for multi-species flow.

The XDEM-Dynamics module is used to predict the motion of solid particles based on Newton's Second Law for conservation of linear and angular momentum

$$m_i \frac{d^2\,\vec{r}_i}{dt^2} = \sum_{i=1}^{N} \vec{F}_{ij}\left(\vec{r}_j, \vec{v}_j, \vec{\phi}_j, \vec{\omega}_j\right) + \vec{F}_{\text{extern}} \tag{13}$$

$$\bar{I}_i \frac{d^2\,\vec{\phi}_i}{dt^2} = \sum_{i=1}^{N} \vec{M}_{ij}\left(\vec{r}_j, \vec{v}_j, \vec{\phi}_j, \vec{\omega}_j\right) + \vec{M}_{\text{extern}} \tag{14}$$

where $\vec{F}_{ij}\left(\vec{r}_j, \vec{v}_j, \vec{\phi}_j, \vec{\omega}_j\right)$ and $\vec{M}_{ij}\left(\vec{r}_j, \vec{v}_j, \vec{\phi}_j, \vec{\omega}_j\right)$ are the forces and torques acting on a particle i of mass m and $\bar{I}_i$ is the tensor moment of inertia. Equations (13) and (14) show that forces and torques exerted on particle i depend on the position $\vec{r}_j$, velocity $\vec{v}_j$, orientation $\vec{\phi}_j$, and angular velocity $\vec{\omega}_j$ of its neighbor particles j. External forces may be include by moving grate bars, fluid forces and contact forces between particles in contact with a bounding wall. Within the XDEM-Dynamics module, forces within particles are present only during mechanical contact. The repulsive force between particles in contact are calculated based on the rigidity of the particles. The interaction between particle-particle and particle-wall is calculated by the contact model linear spring-dashpot and the fluid drag force by the Di Felice's correlation [25].

In the present formulation the deformation of two particles in contact is approximated by its overlapping [11]. The resulting force $\vec{F}_{ij}$ due to contact is calculated by its normal and tangential components

$$\vec{F}_{ij} = \vec{F}_{n,ij} + \vec{F}_{t,ij} \tag{15}$$

where the normal n and tangential t components additionally depend on displacements and velocities normal and tangential to the point of impact between the particles.

The XDEM conversion and dynamics modules are coupled to an implemented CFD solver in OpenFoam for compressible porous media. The last is based on the PIMPLE (PISO-SIMPLE) solution for time-resolved and pseudo-transient simulations allowing equation under-relaxation for better convergence of the equations at each time-step [26]. The CFD equations are the set of the Navier-Stokes equations comprising the mass, momentum, and energy equations for multi-species flow adapted for a porous media [19, 27]

$$\frac{\partial(\epsilon_f\,\rho_f)}{\partial t} + \nabla\cdot(\epsilon_f\,\rho_f\,v_f) = \dot{m}_{s,f} \tag{16}$$

$$\frac{\partial(\epsilon_f\,\rho_f^K\,v_f)}{\partial t} + \nabla\cdot(\epsilon_f\,\rho_f\,v_f\,v_f) = \nabla\cdot(\epsilon_f\,\tau_f) - \frac{\mu_f}{K}\epsilon_f^2\,v_f - C\,\rho_f\,\epsilon_f^3\,|v_f|\,v_f \tag{17}$$

$$\frac{\partial(\epsilon_f\,\rho_f\,h_f)}{\partial t} + (\epsilon_f\,\rho_f\,v_f\,h_f) = \frac{\partial p_f}{\partial t} + \epsilon_f\cdot v_f\cdot\nabla p_f + \sum_{i=1}^{M}\frac{S_p}{V_{REV}}\alpha\Delta T_i \tag{18}$$

$$\frac{\partial(\epsilon_f\,\rho_{f,i})}{\partial t} + \nabla\cdot(\epsilon_f\,\rho_{f,i}\cdot v_f) = \sum_{i=1}^{M} m'''_{s,f,i} \tag{19}$$

The porous media formulation is based on an averaging process over a Representative Elementary Volume (REV) approach [28, 29]. The momentum equation, Eq. (17), is expressed in the formulation for a gas flow within a porous media [19, 27] where K represents the permeability of the packed bed and C the dimensionless drag coefficient. For spherical particles of diameter D_p, K and C can be obtained from [19, 17]

$$K = \frac{D_P^2\epsilon_f^3}{150(1-\epsilon_f)^2} \tag{20}$$

$$C = \frac{1.75(1-\epsilon_f)}{D_P\epsilon_f^3} \tag{21}$$

The intensity of heat exchange between the solid and fluid phases in the energy equation (Eq. (18)) is subjected to the thermal boundary conditions at the interface where S_p is the heat source term responsible for transferring the thermal energy from the fluid to the particles and/or from the particles to the flow

$$S_p\, h_{p,f}(\Delta T_p) = q'''_{sf}\, V_{REV} \tag{22}$$

The last term of the right hand side in Eq. (18) represent the coupling between DPM and CFD for heat transfer simulations.

Simulation Domain and Boundary Conditions

A cylindrical shape can be used to represent the geometry of a generic reactor. In the present case, the generic geometry is further simplified by considering one quarter of it filled with particles. The two investigated geometries are shown in Figs. 3 and 4. The computational domain 1 shown in Fig. 3 is used to study chemical conversion by employing the XDEM-Conversion module. The dimensions of this domain are 300 mm in height with a radius of 225 mm. The domain is discretized with a structured grid which contains 3176 cells with an average size of 20 mm × 22 mm × 22 mm. The second geometry is presented in Fig.4. This geometry is used to study the motion of the particles around the gas injection as well as the heat-up process due to the hot gas. The dimensions of this domains are 800 mm in height with a radius of 400 mm. The domain contains 9144 cells with an average size of 25 mm × 25 mm × 23 mm. Both computational domains are bounded by two side-walls, an outer wall which shapes the cylindrical form of the reactor, an inlet, an outlet (top wall) and a bottom wall. The inlet (showed in solid color) is located at center of the outer wall. In geometry 1 (Fig. 3) is located one cell above the bottom wall whereas in geometry 2 (Fig. 4) is placed at the third cell above the bottom wall. The packed bed is represented by an ensemble of particles with an inhomogeneous void space between them due to their packing. Each sphere has a diameter of 20 mm and is considered to be a coke particle. The coke particles are at rest and randomly settled at the bottom of the cylinder. This was done in a preliminary simulation by placing the particles at the center of the domain and let them fall until they reached their random and steady position. The computational domain in Fig. 3 contains 300 coke particles where as the domain in Fig. 4 contains 3000 particles. Coke properties are shown in Table 1. Hot air at 1200 K in a standard mass fraction composition, $Y_{O_2} = 0.21$ and $Y_{N_2} = 0.79$, is injected through the inlet at a velocity of $u = 20\,\mathrm{m\,s^{-1}}$. For simplicity the inflow profile is considered to be uniform. For the side-walls a cyclic boundary condition is used. At the outlet (top wall), the conservative variables are simply extrapolated from the inside domain. An initial temperature of 600 K is set for the gas and the particles. Temperature is extrapolated from the inside domain to the walls. The standard $k - \epsilon$ model is used with an initial turbulence values set to 3 %.

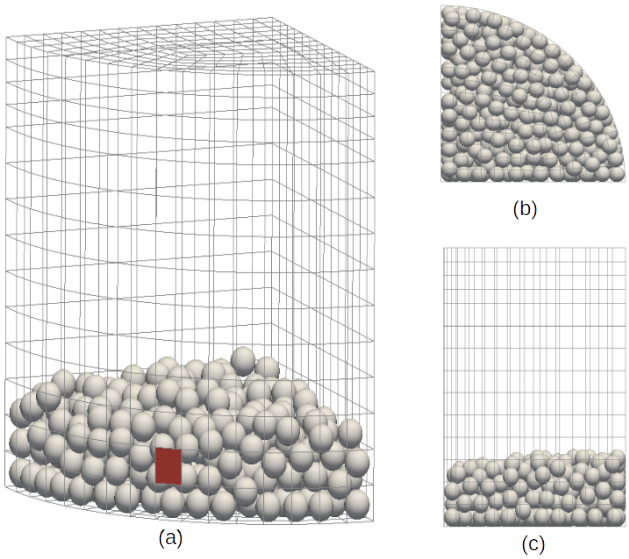

Figure 3: Geometry 1 with 300 particles, different views of the computational domain: (a) isometric, (b) top, and (c) lateral.

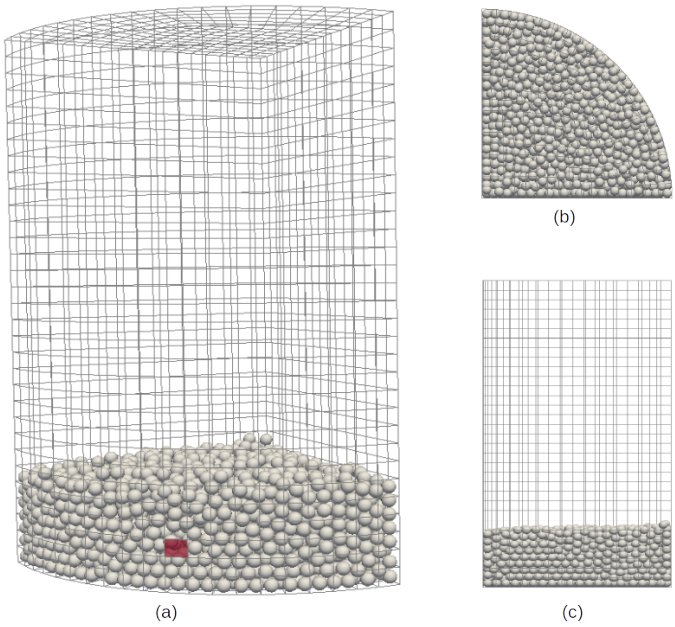

Figure 4: Geometry 2 with 3000 particles, different views of the computational domain: (a) isometric, (b) top, and (c) lateral.

Table 1: Thermodynamic and mechanical properties of coke.

Density [kg/m^3]	1050	Young modulus [Pa]	22×10^9
Porosity [-]	0.2	Poisson ratio [Nm^{-1}]	0.3
Tortuosity [-]	1.0	Friction coefficient [-]	1

Results and Discussion

The XDEM has been validated for spherical particles of diverse materials by comparing predicted and experimental results [16]. For instance, Fig. 5 shows the experimental and predicted data for gasification of spherical char particles of 10 mm and 15 mm diameter exposed to a heating temperature of 773 K. The measurements were obtained from experiments conducted by Schäffer and Wyrsch [30]. The comparison between the measured and predicted reduction in the particle mass fraction shows a good agreement. The particle mass fraction and radius decreases linearly indicating a shrinking behavior. The high char reactivity limits the reaction regime and the transfer of oxygen through the boundary layer represents the rate-limiting step [16]. Therefore, the obtained agreement shows that heat and mass transfer are evaluated with sufficient accuracy.

For the present test-case, the gasification of coke particles inside the reactor is approximated by the following reaction

$$C + \frac{1}{2}O_2 \leftrightarrow CO \tag{23}$$

As observed from Fig. 5 gasification occurs if the particle is exposed to a heating temperature for a considerable amount of time. In terms of simulation this represents a large computational time. In order to account for gasification effects and to test the XDEM capability while simulating multiple particles, the simulation domain shown in Fig. 3 is used. Since large exposure of time is required to observed the heating up and gasification processes, an static simulation using only the XDEM-Conversion module and the CFD coupling is computed first. Accordingly, the governing equations for the flow and particles are solved taking into account conduction between particles and the surrounding flow field. Deactivating the XDEM-Dynamics module allows to increase the time step and achieve a faster solution accounting for heat and mass transfer within the particles and gas, while keeping the particles static. Figure 6 shows the predicted heat-up of the packed bed via the temperature distribution at surface of the particles and in the flow. The increase in temperature can

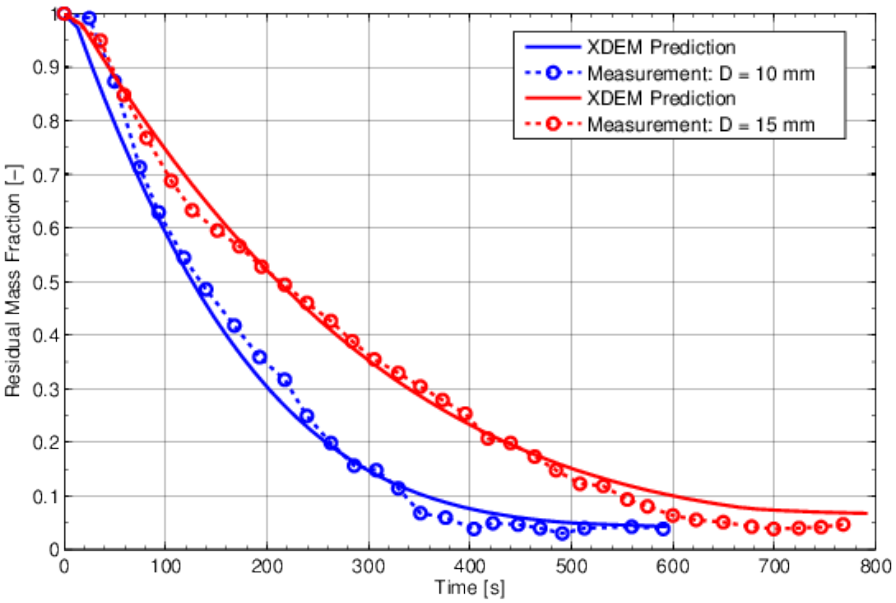

Figure 5: Comparison between measurements and predictions for gasification of char particles of 10 mm and 15 mm diameter exposed to a heating temperature of 773 K [16].

be observed through different instants in time. At the initial time, $t = 0$ s, the temperature of the domain is given by the ambient conditions $T = 600$ K. As air is injected through the inlet, the hot stream at $T = 1200$ K heats up the particles and the ambient air. The heat propagation can be appreciated through the different instants in time $t = 120$ s, $t = 400$ s, and $t = 800$ s. The particles located in front of the inlet are the first to receive the blast of hot air and to rise its temperature. The hot air moving through the void space of the packed bed continue heating up the particles. As observed from Fig. 6, the heat propagates from the inlet towards the side-walls and to the center of the reactor. At the last time, $t = 800$ s, temperatures over 1000 K are reached, principally at the particles located around the inlet. The CO concentration in the flow and the shrinking of the particles are the result of gasification, heat and mass transfer between the solid and gas phases. The carbon and oxygen react to form CO according to Eq. (23) just after the necessary temperature to activate the reaction has been reached. CO is then transported through the void space of the packed bed and to the flow above the particles. The effects of gasification are visible by the decrease in the diameter of the particles and the production of CO at $t = 800$ s, Figs. 7 and 8. A mass fraction reduction of approximately 20 % is observed at the particles that are directly located at the inlet and have been exposed to a longer heating period, $t = 800$ s.

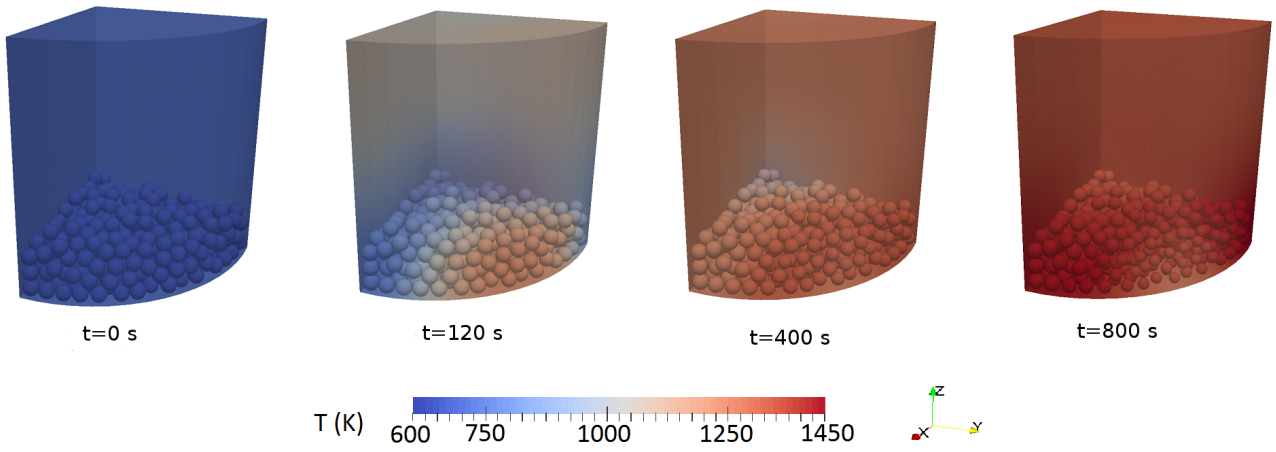

Figure 6: Temperature distribution at the particles surface and the flow field at different times.

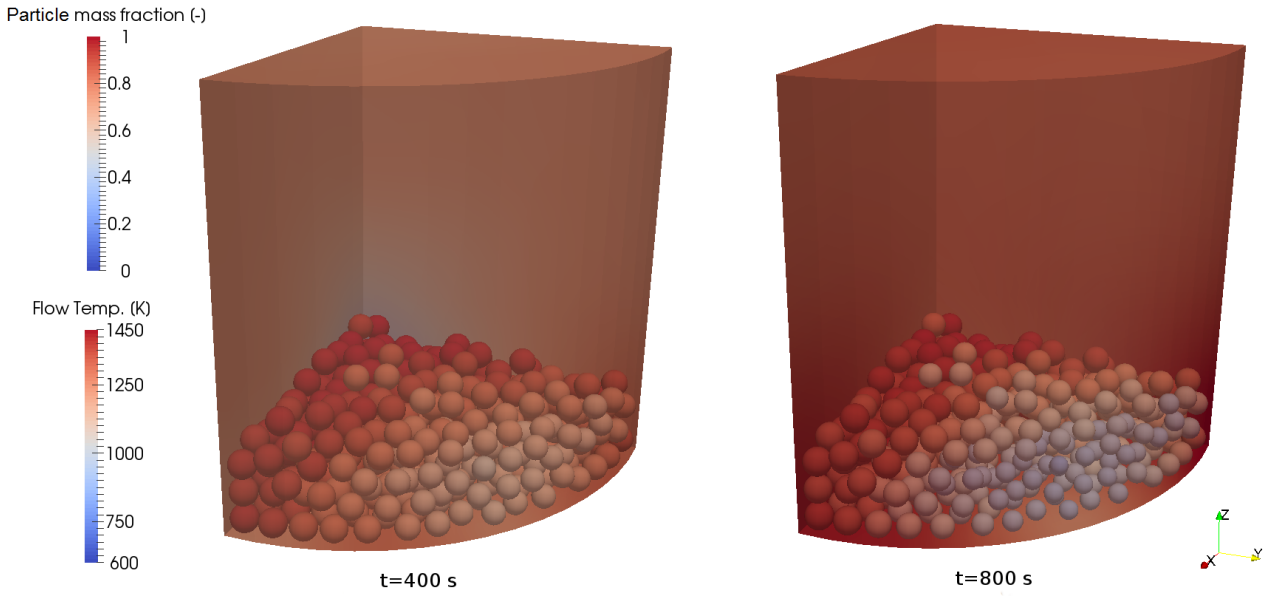

Figure 7: Particle mass fraction and flow temperature distribution in the reactor.

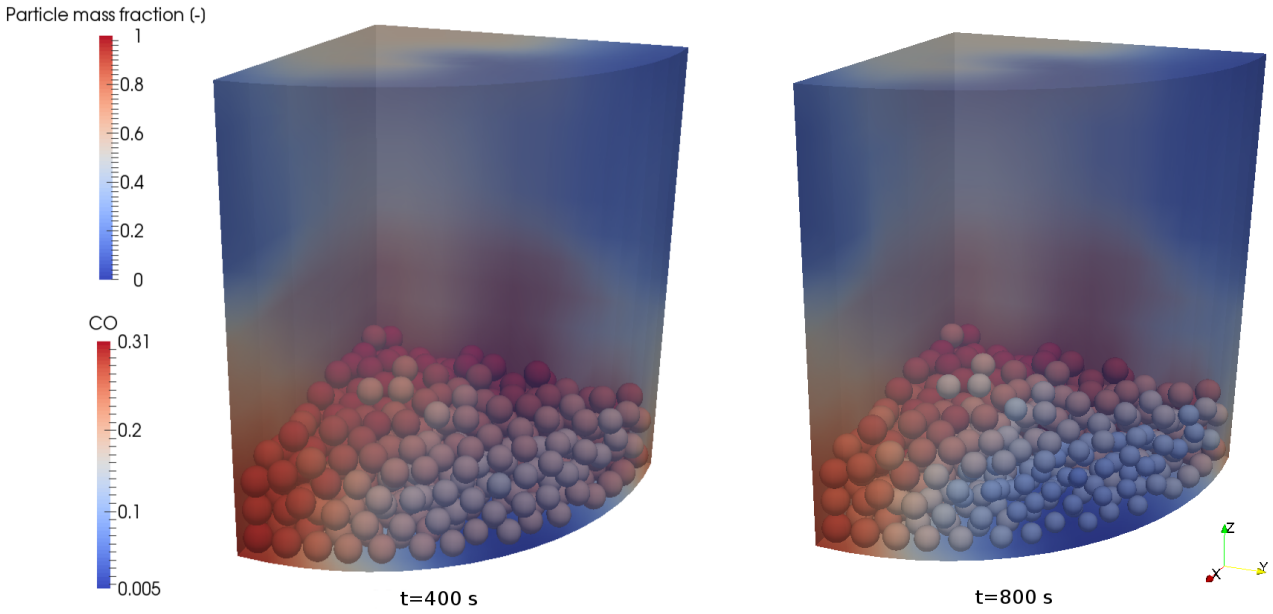

Figure 8: Particle mass fraction and CO concentration.

The XDEM-Dynamics module is used to account for the motion of the coke particles. A combination of the conversion and dynamics modules coupled with the CFD gas phase allows the XDEM to predict the motion and chemical conversion of each particle. The computational domain shown in Fig. 4 is used to simulate the motion of the coke particles inside the reactor by using the XDEM-Dynamics. Since the particles are also exposed to hot air, chemical conversion is solved with the conversion module. As observed from the previous case, gasification of coke particles require large exposure time to a heating source. This results in highly computational costs. In order to avoid such large computing time, the following test-case runs for a simulation time of 10 s. This time is enough to analyze the motion of the particles and the the heat-up process. Based on the previous case it is assumed that if the run time were increased, gasification process would take place. Figure 9 shows the temperature distribution in the flow and at the surface of the particles. Streamlines colored by the flow temperature are displayed to better visualize the flow going through the particles and the reactor. From Fig. 9 it

can observed how the injected flow at $T = 1200\,\mathrm{K}$ progressively heats-up the particles. Right after the injection, $t = 0.2\,\mathrm{s}$, the hot jet penetrates through the packed bed pushing forward the particles. Due to the packing of the particles and the location of the inlet, the jet immediately impacts on the solid bodies and it divides in two main streams. One stream continues in direction to the center of the reactor and the other continues in radial direction around the outer-walls. The particles located in front and around the inlet are pushed back and upwards by the stream traveling to the center.

The inject hot gas moves through the void space of the packed bed transferring its thermal and kinetic energy to particles. As it can be observed from Fig. 9 the streamlines represent the increase of the temperature in the flow field from the initial time $t = 0\,\mathrm{s}$ up to $t = 10\,\mathrm{s}$. Most of the thermal energy contained in the injected gas is absorbed by the particles. As the time increases the heat-up in the particles is more visible. As expected, the particles that are exposed directly to the hot gas are the first to heat-up and reach the highest temperatures. Figure 9 also shows the temperature at the surface of the particles. From the ambient condition, $T = 600\,\mathrm{K}$, it takes around 10 seconds to heat-up few particles to a more than 1000 K. Since the particles are moving and changing location not all of them close to the inlet show the same the temperature. However, the particles with larger temperatures are located around the inlet.

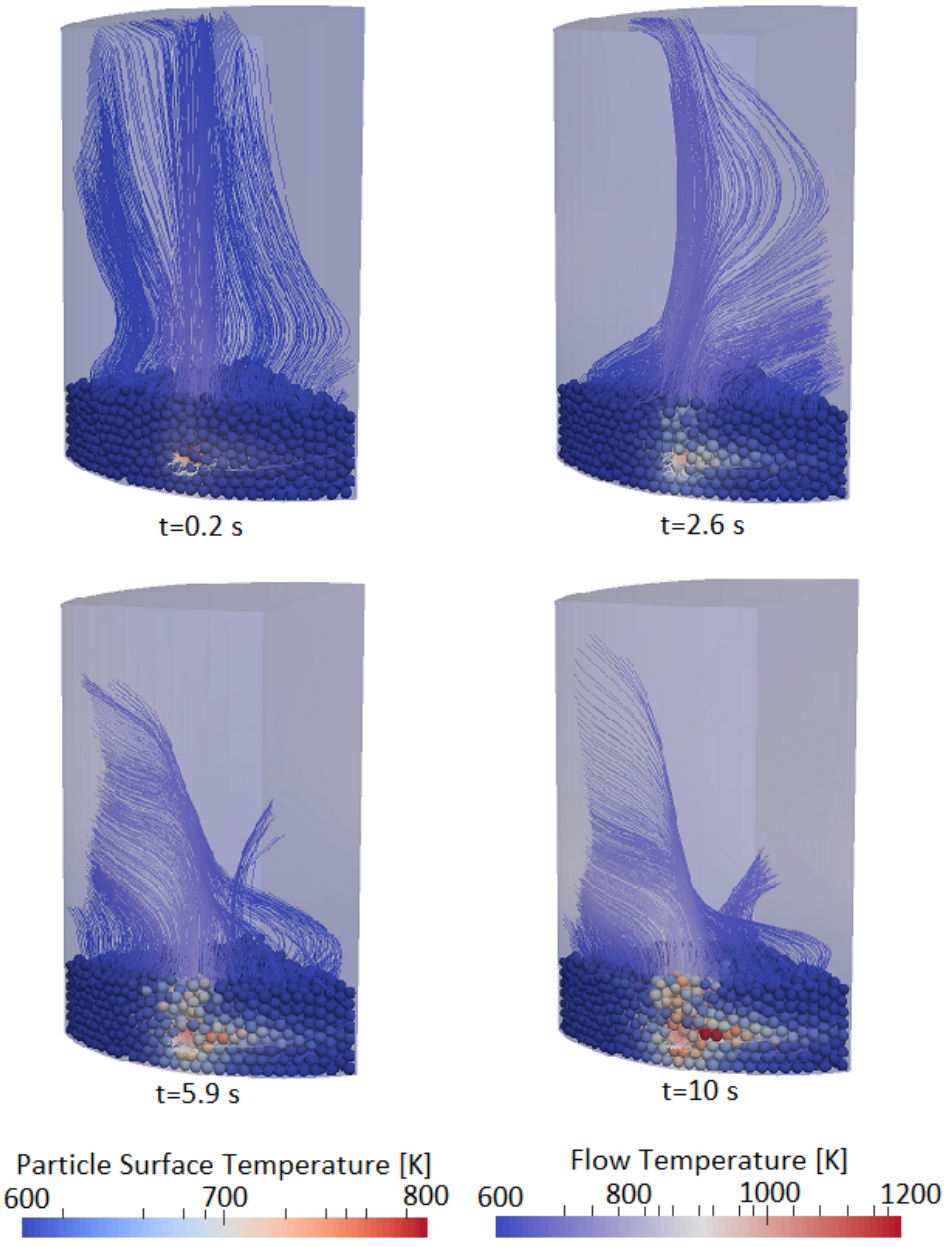

Figure 9: Temperature distribution in the flow field and at the particles surface at different times.

The air injected into the packed bed generates a circulation region with the particles moving around of it. This can be appreciated in Fig. 10 where a close-up around the inlet is shown. At the initial time, $t = 0\,\mathrm{s}$, the particles are static inside the reactor. When the air is injected at $u = 20\,\mathrm{m\,s}$ the particles located right at the inlet are pushed inwards. As the air continue penetrating into the packed bed, the particles are further displaced towards the center leaving a small cavity occupied only by the incoming air. Due to the displacement of these particles and the jet penetrating deeper into the packed bed and displacing more entities. The particles above this layer fall into the cavity to fulfill the free space. Since air is supplied continuously, the particles falling into the cavity and then been pushed inwards is repeated. Since the air speed is not large enough to penetrate deeper and push the particles further towards the center, these particles are rotating around the incoming air as shown in Fig. 11. The effect of the injected air into the particles extends up to approximately one third of the radius of the cylindrical reactor, 130 mm. It seems that the momentum of the jet is not enough to significantly displace the particles located beyond this distance. However, the thermal energy of the jet is enough to heat-up those particles. The rotational movement of the particles located near the inlet is responsible for the non uniform temperature distribution observed in Fig. 9. In particular, the particles with higher temperatures are located above and below the inlet due to this vertical rotational movement. The formation of the cavity and the recirculation region around the jet is a common pattern to be expected in such typed of gas-particle beds [31, 32].

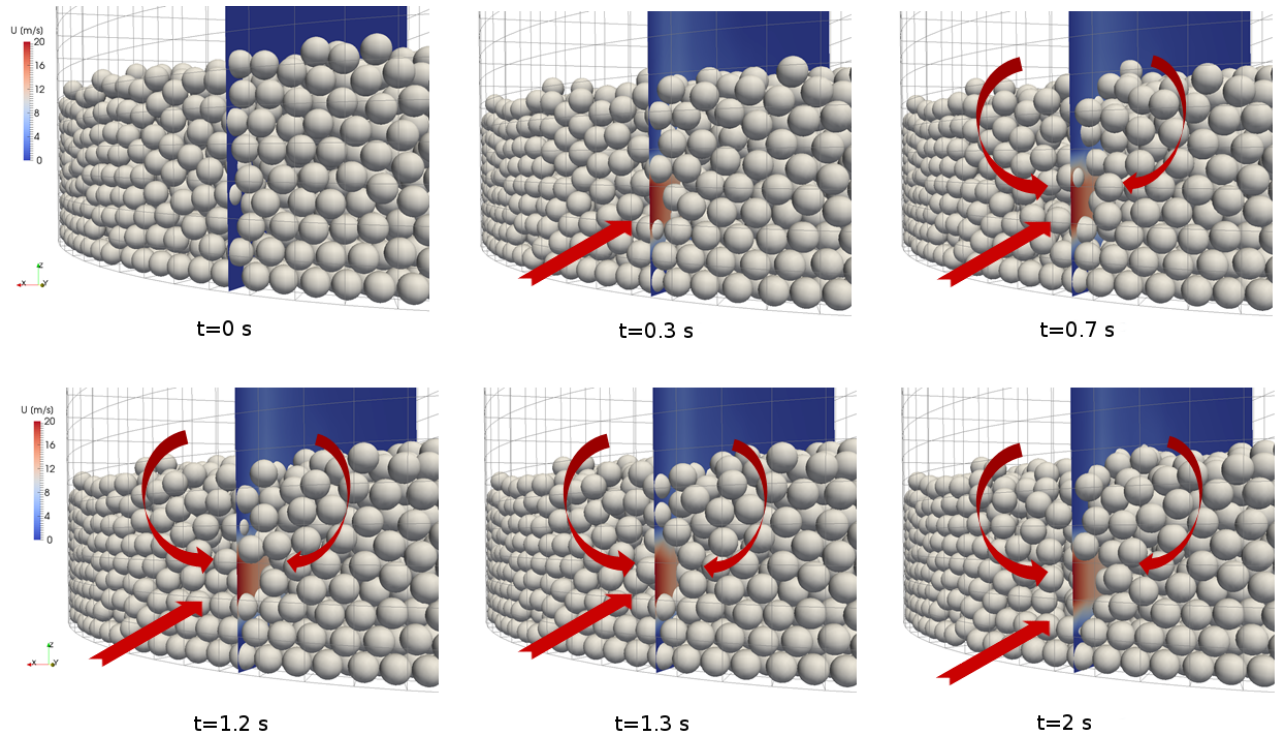

Figure 10: Velocity distribution and displacement of the particles around the inlet.

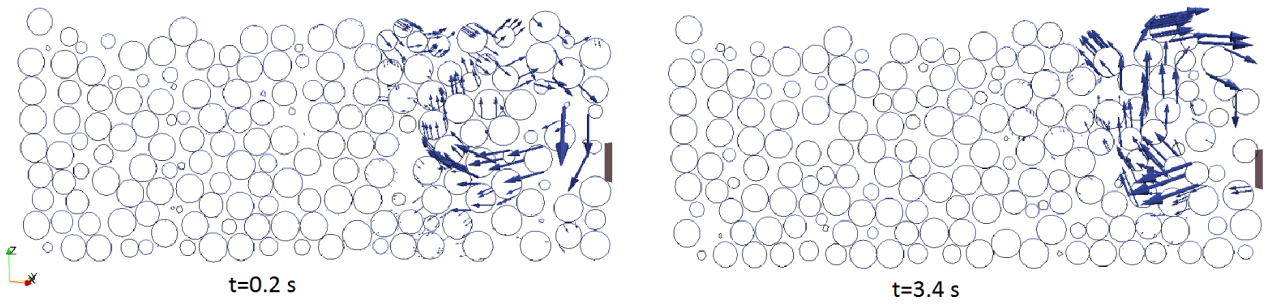

Figure 11: Velocity vector indicating the trajectory of the particles. 2D-cut at the cross-section in front of the inlet.

Conclusions

In the present case-study the developed numerical framework eXtended Discrete Element Method (XDEM) has been used to simulate the injection of gas into a packed bed of particles. The XDEM conversion and dynamics modules coupled to an implemented CFD solver in OpenFoam have been used to account for the motion and chemical conversion of particles subject to lateral gas injection. In a first step, the XDEM-Conversion module was validated for a single coke particle exposed to a heating source. The available experimental data was compared with the predicted values for the reduction of mass fraction and the particle diameter. Since good agreement between the measured and predicted values was obtained, the XDEM-Conversion was applied to a multiple coke particles to predict the heat-up and gasification process. The results shown how the particles shrink and loss their mass as the heating time increases. Due to the internal reaction part of the mass of the coke particles was transformed into CO and transported into the flow. The XDEM conversion and dynamics modules together with the CFD solver were used to predict the motion of the particles exposed to the lateral gas injection. In this case, the expected formation of a cavity and circulating region around the gas was observed. The transfer of thermal energy from the hot gas to the particles was observed by the increase in the temperature of the particles. The circulating region was also confirmed by the temperature distribution within the packed bed. The XDEM showed the ability to predict the motion and chemical conversion of particles in a packed bed subject to lateral gas injection. However, for better representation of the case in a real industrial application, such as a blast furnace, it is necessary to account for more realistic geometries and boundary conditions.

Acknowledgments

The authors would like to thank the Luxembourg National Research Foundation (FNR) for the support of this project.

References

[1] Adema, A. (2014) DEM-CFD Modelling of the ironmaking blast furnace. *PhD Thesis* TU Delft, The Netherlands.

[2] Geerdes, M., Toxopeus, H., van der Vliet, C., Chaigneau, R., and Vander, T. (2009) Modern Blast Furnace Ironmaking: An Introduction. *IOS Press*.

[3] Mathieson, J. G., Truelove, J. S., and Rogers, H. (2005) Toward an understanding of coal combustion in blast furnace tuyere injection. *Fuel* **84(10)**, 1229-1237.

[4] Burgess, J. M. (1985) Fuel combustion in the blast furnace raceway zone. *Progress in Energy and Combustion Science* **11(1)**, 61-82.

[5] Khairil, K., Kamihashira, D., and Naruse, I. (2002) Interaction between molten coal ash and coke in raceway of blast furnace. *Proceedings of the Combustion Institute* **29(1)**, 805-810.

[6] Peters, B., Dziugys, A., and Navakas, R. (2012) A shrinking model for combustion/gasification of char based on transport and reaction time scales. *Mechanika* **18(2)**, 177-185.

[7] Gidaspow, D. (1994) Multiphase Flow and Fluidization: Continuum and Kinetic Theory Descriptions. *Academic Press*

[8] Kuipers, J. A. M., and van Swaaij W. P. M. (1997) Application of Computational Fluid Dynamics to Chemical Reaction Engineering. *Reviews in Chemical Engineering*.

[9] Xu, B. H., and Yu, A. B. (1998) Comments on the paper numerical simulation of the gas-solid flow in a fluidized bed by combining discrete particle method with computational fluid dynamics - reply. *Chemical Engineering Science*. **53(2)**, 2646-2647.

[10] Peters, B. (2013) The extended discrete element method XDEM for multi-physics applications. *Scholarly Journal of Engineering Research* **2(1)**, 1-20.

[11] Cundall, P. A. and Strack, O. D. L. (1979) A discrete numerical model for granular assemblies. *Geotechnique* **29**, 47-65.

[12] Gallas, J. A. C., Herrmann, H. J., and Sokolowski, S. (1992) Convection cells in vibrating granular media. *Physical Review Letters* **69(9)**, 1371-1374.

[13] Walton, O. R. and Braun, R. L. (1986) Viscosity, granulartemperature, and stress calculations for shearing assemblies of inelastic, frictional disks. *Journal of Rheology* **30(5)**, 949-980.

[14] Džiugys, A. and Peters, B. (2001) An approach to simulate the motion of spherical and non-spherical fuel particles in combustion chambers. *Granular Matter* **3(4)**, 231-266.

[15] Mahmoudi, A. H., Hoffmann, F., and Peters, B. (2014) Application of XDEM as a novel approach to predict drying of a packed bed. *International Journal of Thermal Sciences* **75**, 65-75.

[16] Peters, B. (2003) Thermal Conversion of Solid Fuels. *Internal Series on Developments in Heat Transfer, WIT press*

[17] Peters, B., Dziugys, A., and Navakas, R. (2010) A discrete approach to thermal conversion of solid fuel by the discrete element method (dpm). *Modern Building Materials, Structures and Techniques*

[18] Mahmoudi, A. (2015) Prediction of Heat-up, Drying and Gasification of Fixed and Moving Bed by the Discrete Particle Method (DPM). *PhD Thesis, University of Luxembourg*.

[19] Faghri, A. and Zhang, Y. (2006) Transport Phenomena in Multiphase Systems. *Elsevier Academic Press*

[20] Grønli, M. (1996) A theoretical and experimental study of the thermal degradation of biomass. *PhD Thesis, NTNU Trondheim*.

[21] Shih-I, P. (1977) Two-Phase Flow. *Vieweg Tracts in Pure and Applied Physics*

[22] Dullien, F. A. L. (1979) Porous Media Fluid Transport and Pore Structure. *Academic Press, San Diego*

[23] Peters. B. (1997) Numerical simulation of heterogeneous particle combustion accounting for morphological changes. *27th International Conference on Environmental Systems* **SAE paper 972562**, USA.

[24] Peters, B. (1999) Classification of combustion regimes in a packed bed based on the relevant time and length scales. *Combustion and Flame* **116**, 297-301.

[25] Di Felice, R. (1994) The voidage function for fluid particle interaction system. *International Journal of Multiphase Flow* **20**, 153-159.

[26] OpenFoam User Guide, V.2.0.0. (2011)

[27] Bird, R. B., Stewart, W. E., and Lightfoot E. N. (1960) Transport Phenomena. *John Wiley & Sons.*

[28] Teng, H. and Zhao, T. S. (2000) An extension of Darcy's law to non-stokes flow in porous media. *Chemical Engineering Science* **55**, 2727-2735.

[29] Lage, J. L., Lemos, M. D., and Nield, D. (2002) Transport Phenomena in Porous Media II. *Modeling Turbulence in Porous Media, Pergamon*, **Chap. 8**, 198-230.

[30] Schäffer, B. and Wyrsch, F. (2000) Untersuchungen der Produktzusammensetzung bei thermochemischen Konversionsprozessen von Biomasse. *Diplomarbeit, ETH Zürich, Institut für Energietechnik, LTNT.*

[31] Hilton, J. E. and Cleary, P. W. (2012) Raceway formation in laterally gas-driven particle beds. *Chemical Engineering Science* **80**, 306-316.

[32] Nogami, H., Yamaoka, H., and Takatani, K. (2004) Raceway Design for the Innovative Blast Furnace. *ISIJ International* **44**, 2150-2158.